

Chapter 5

Evaluation of the Transient Performance of Super-Wideband Printed-Circuit Antennas Using Time-Domain Electromagnetics

Marjan Mokhtaari and Jens Bornemann

Abstract A time-domain electromagnetics code is used to evaluate the transient and radiation performances of three printed-circuit antennas for super-wideband (SWB) monitoring applications. For two antennas, one in microstrip and one in coplanar technologies, operating between 3 and 30 GHz with a return loss of 10 dB, it is demonstrated that the vertically polarized omnidirectional radiation characteristics in the lower frequency band change to a more directional pattern at higher frequencies and that the cross-polar field component increases with frequency and gives rise to possible dual-polarized applications for the microstrip antenna. In comparison, the coplanar antenna shows slightly better performance, especially with respect to its transient response. Its group-delay variation is only 180 ps compared to 250 ps of the microstrip antenna, and its amplitude response provides better polarization purity. The evaluation of the coplanar concept is extended to cover a bandwidth between 3 and 60 GHz. The time-domain evaluation, as validated by a frequency-domain technique, demonstrates that bandwidths in extent of decade bandwidths are possible with simple printed-circuit antennas. Characteristics and performances are presented for possible applications in future SWB monitoring systems, radar technology, through-wall imaging systems, and other future wireless services. Antenna dimensions are provided for future comparisons with improved and/or multi-level electromagnetics codes.

Keywords Antenna · Microstrip · Ultra wide band (UWB) · Coplanar waveguide · Polarization · Time domain

M. Mokhtaari · J. Bornemann (✉)
Department of Electrical and Computer Engineering, University of Victoria,
Victoria, BC V8W 3P6, Canada
e-mail: j.bornemann@ieee.org

5.1 Introduction

Applications of time-domain electromagnetics and related codes have significantly increased since 2002, when the ultra-wideband (UWB) frequency spectrum between 3.1 and 10.6 GHz was released by the US Federal Communications Commission (FCC). UWB technology operates with electromagnetic pulses, which are spread over a wide frequency spectrum and transmitted at low power levels not exceeding effective isotropic radiated power (EIRP) density levels of -41.3 dBm/MHz. The transmission principle, which is based on pulses between a few tens of picoseconds and a few nanoseconds, representing a single or a few cycles of a radio-frequency carrier waveform, is ideally suited for transient analysis by time-domain electromagnetics codes. For such applications, they present distinct advantages over frequency-domain techniques, mostly in terms of computation time and efficiency. Fourier transforms are usually performed to present the data in the frequency domain.

As small antennas form a fundamental requirement for UWB systems, a large number and variety of printed-circuit antennas to cover this frequency range have been proposed. For such a bandwidth, the ratio between upper and lower frequencies is 3.4:1. However, it was found later that the bandwidths of some UWB antennas could be extended to approximately 30 GHz, thus providing a bandwidth ratio of 10:1 and inspiring the term “super-wideband (SWB) antennas.”

As applications of wireless data transmission are increasing in number and in frequency, e.g., up to 60 GHz [1], an obvious need for proper monitoring equipment arises in order to enforce standards or investigate related topics. The range of sensor and monitoring applications is widespread and addresses issues such as EIRP compliance [2], immunity tests [3], interference [4], high-power microwave detection [5], health-related testing [6, 7], and many more.

In order to detect electromagnetic emissions in such a wide range of frequencies and applications, equipment must have SWB performance. Thus, associated systems for testing, sensing, and monitoring are developed. Sensor networks for wireless applications have been proposed, e.g., [8], and EMC testing equipment for mobile phones is being developed, e.g., [9]. Recently, a system for EMI measurements up to 26 GHz was presented [10].

Within such testing systems, the UWB or SWB antenna is of paramount importance as it must provide the bandwidth for an often multiband receiver system. TEM horns can be used in chamber measurement setups, e.g., [11], for initial tests and certification procedures. For mobile monitoring, however, printed-circuit antennas are more appropriate. Hence, a large number of printed-circuit antennas have been developed within the last several years, e.g., [12, 13].

However, many designs are confined to the 3–10 GHz range for compliance with the FCC approved bandwidth. Only rarely and more recently have monopole-type antennas been presented that extend the applicable frequency range to 20 GHz [14], 30 GHz [15], 40 GHz [16], 50 GHz [17], 60 GHz [18] and, although without verification, up to 150 GHz [19]. Common to most of these antennas is a

printed-circuit monopole whose return loss has been optimized to cover a much larger band than the original 3–10 GHz range, but whose change in transient behavior and pattern characteristics over the much wider band has been accepted as unavoidable.

This chapter presents the time-domain evaluation for the transient performance of SWB printed-circuit antennas. Three planar antennas, one in microstrip and two in coplanar waveguide (CPW) technology are analyzed. Following the presentation of a general design procedure for such antennas in Sects. 5.2 and 5.3 introduces the transient evaluation of a microstrip and a CPW antenna for SWB applications with capabilities up to 30 GHz, thus covering not only the 3.1–10.6 GHz UWB range, but also that for vehicular radar between 20 and 29 GHz. Their geometries are similar to 3–10 GHz UWB antennas, but their frequency range has been significantly increased. Section 5.4 presents the analysis of a second coplanar antenna whose bandwidth is extended to cover the 3–60 GHz range, thus providing a bandwidth ratio of 20:1.

5.2 General Antenna Design Procedure

The vast majority of published printed-circuit UWB antennas consist of a microstrip-line-fed metalized and arbitrarily shaped patch over a removed ground plane. In order to provide the bandwidth for SWB antennas and/or extend the existing UWB antennas to much higher frequencies, the following optimization process is adopted.

Our design procedure starts with a hexagon whose corner points are located on a circle (Fig. 5.1a). The feed is assumed to be connected at point P_0 , and can be either in microstrip or coplanar technology. The coordinate system adopted in this work is shown in Fig. 5.1b. If a microstrip line is used, as shown in Fig. 5.2a, the ground plane is abruptly terminated, thus creating a patch that represents a monopole over a horizontal ground plane. In CPW technology (Fig. 5.2b), the ground planes on either side of the center conductor are sloped in the same way as the radiating monopole. At higher frequencies, this can be viewed as a linearly tapered slot antenna (LTSA) whose radiation characteristics are mainly in the direction indicated by $\theta = 90^\circ$ and $\phi = \pm 90^\circ$.

For the design and evaluation procedure, the time-domain solver of CST Microwave Studio is used. For the extremely large bandwidths involved in this work, time-domain analysis, as opposed to a frequency-domain solution, has turned out to present a tremendous advantage in terms of CPU time, and thus timeliness in an actual design exercise. An SWB pulse in the respective frequency range is applied to the input of the microstrip (or CPW) line at P_0 (Fig. 5.1a), and positions P_1 , P_2 , and P_3 are varied. Symmetry of the radiating patch is enforced, thus determining points P'_1 , P'_2 . The time-domain reflected wave at P_0 is Fourier transformed and the reflection coefficient monitored over a wide frequency range. The optimization is terminated when the reflection coefficient at P_0 is at or lower

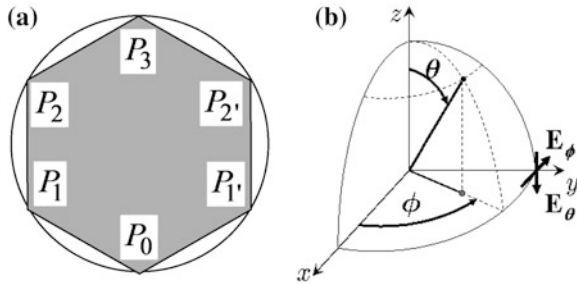


Fig. 5.1 Initial geometry of the UWB/SWB antenna (a) with point P_0 indicating the feed by either a microstrip line or coplanar waveguide, and the coordinate system (b) adopted in this work

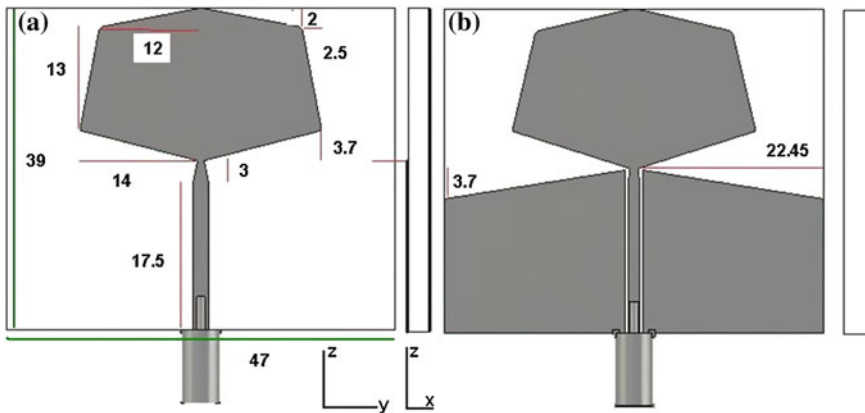


Fig. 5.2 Layouts, dimensions (in mm), and coordinate system of printed-circuit 3–30 GHz SWB antennas in microstrip (a) and CPW (b) technologies

than -10 dB. Note that the feeding coaxial cable is included in all simulations as it presents, first, a nonnegligible reflection at its interface to the printed-circuit board and, secondly, connects the two ground planes in the CPW design (Fig. 5.2b).

5.3 Evaluation of 3–30 GHz Antennas

As mentioned before, the transient evaluation method used here is based on a short pulse that is excited at the input of the coaxial cable feeding the antenna (c.f. Fig. 5.2). The reflected pulse is monitored and the ratio of Fourier transforms of reflected to transmitted pulse is displayed as the reflection coefficient versus frequency. For pattern computation, a radiation boundary, e.g., [20], is defined from

which far field radiation patterns can be extracted. The transient performance is evaluated by placing a probe in the far field of the antenna and Fourier transforming the input pulse at the coaxial cable and that received at the far-field probe. The ratio of amplitudes is displayed as amplitude response versus frequency. The phase information is shown as group delay, which is the derivative of the phase difference w.r.t. angular frequency.

The microstrip and coplanar antennas for 3–30 GHz SWB applications are shown in Fig. 5.2a, b with their respective dimensions. The substrate is selected as RT/Duroid 6002 with $\epsilon_r = 2.94$, $\tan\delta = 0.0012$, substrate height of 0.762 mm and metallization thickness of 17.5 μm . The characteristic impedances of the feeding microstrip and coplanar transmission lines are 50 Ω , and a 40 GHz coaxial cable is chosen to feed the antennas.

Figure 5.3a shows the reflection coefficients of both the microstrip and CPW antennas. Between 2.8 and 30 GHz, $|S_{11}|$ is less than -10 dB, thus validating the time-domain design procedure to obtain a broadband match. The influence on the substrate material, both in terms of permittivity and substrate height and at the example of the microstrip antenna (Fig. 5.2a), is depicted in Fig. 5.3b. It is observed that the reflection coefficient decreases with decreasing permittivity and decreasing substrate height. This result is later used to design the SWB antenna up to 60 GHz.

Figure 5.4a, b shows the E-plane radiation characteristics of the microstrip antenna for 14 different frequencies. It is obvious that in the lower frequency range, the antenna behaves like a typical monopole, whereas toward higher frequencies, the number of minima increases due to the reducing wavelength. These tendencies are corroborated by the H-plane patterns (Fig. 5.4c, d) that show nearly omnidirectional characteristics at low frequencies and an increasing number of minima toward higher frequencies. It is noted that although several angles experience minima at different frequencies, the preferred directions of $\theta = 90^\circ$ and $\phi = \pm 90^\circ$ are available throughout the entire SWB frequency range.

Similar observations can be made for the CPW antenna of Fig. 5.2b whose E-plane and H-plane patterns at 14 different frequencies are shown in Fig. 5.5a–d, respectively. The patterns of both antennas, microstrip and CPW, are similar as both antennas change to a more directional characteristic as frequency increases.

A difference in their respective performance can be observed if not only the co-polar E_θ components, as in Figs. 5.4 and 5.5, are displayed, but also in their cross-polar E_ϕ components, which are shown as well. Rather than presenting all cross-polar radiation patterns, we display the responses of the antennas in the preferred direction of $\theta = \phi = 90^\circ$.

The results of the transient analysis are presented here only for a single preferred direction. The analysis over an entire sphere requires transient modeling of a very large structure (due to lowest frequency far-field condition) and use of supercomputing or parallel-processing capabilities.

Figure 5.6 shows the amplitude and group delay plots over the entire frequency range between 1 and 30 GHz. The probe is located at $\theta = \phi = 90^\circ$, which is the right horizontal direction in Fig. 5.2. The low amplitude level in Fig. 5.6a is due to

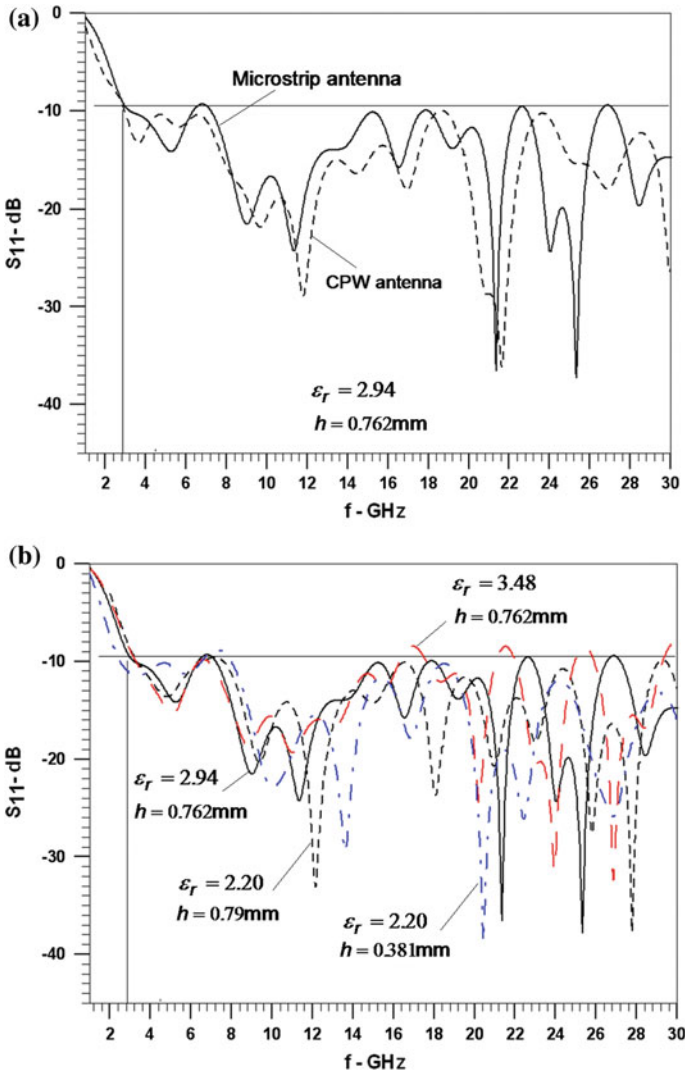


Fig. 5.3 Reflection coefficients in dB of the microstrip (solid line) and CPW (dashed line) SWB antennas (a); changes in the input reflection coefficient for the microstrip antenna (Fig. 5.2a) in terms of substrate material and height (b)

the extremely small size of the probe and its omnidirectional characteristic. While the vertical polarization E_θ of both antennas is wavy, but at a reasonable level over the entire frequency range, the horizontal (cross) polarization E_ϕ increases with frequency and, between 26 and 28 GHz, shows levels in the same order of magnitude for the microstrip antenna. This would permit the use of dual-polarized applications if required, especially since also the group delay (Fig. 5.6b) is almost

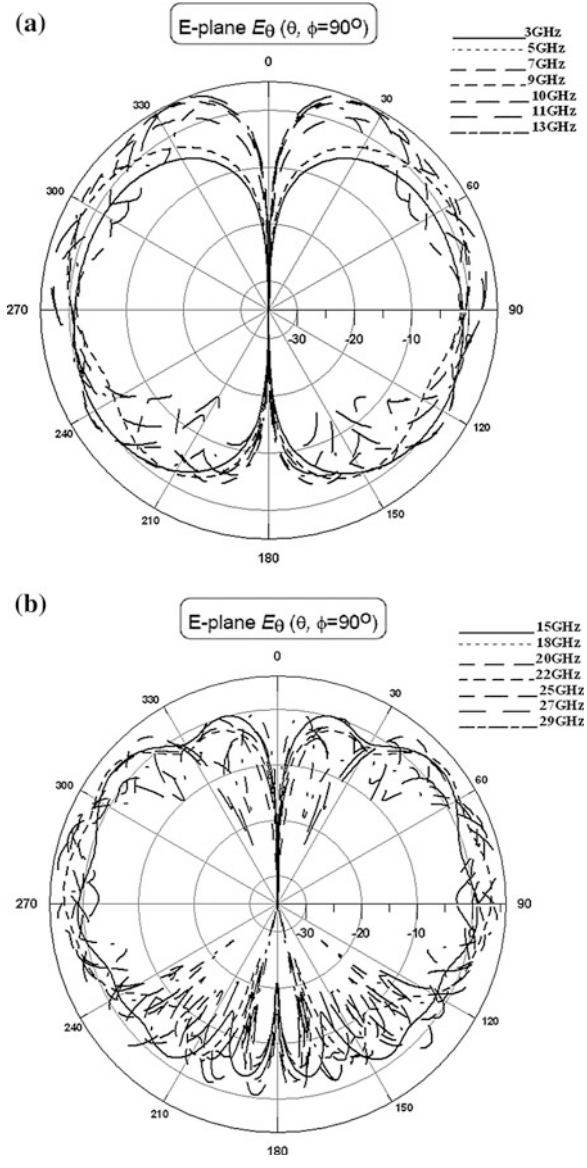


Fig. 5.4 E-plane (a and b) and H-plane (c and d) radiation patterns of the microstrip SWB antenna of Fig. 5.2a

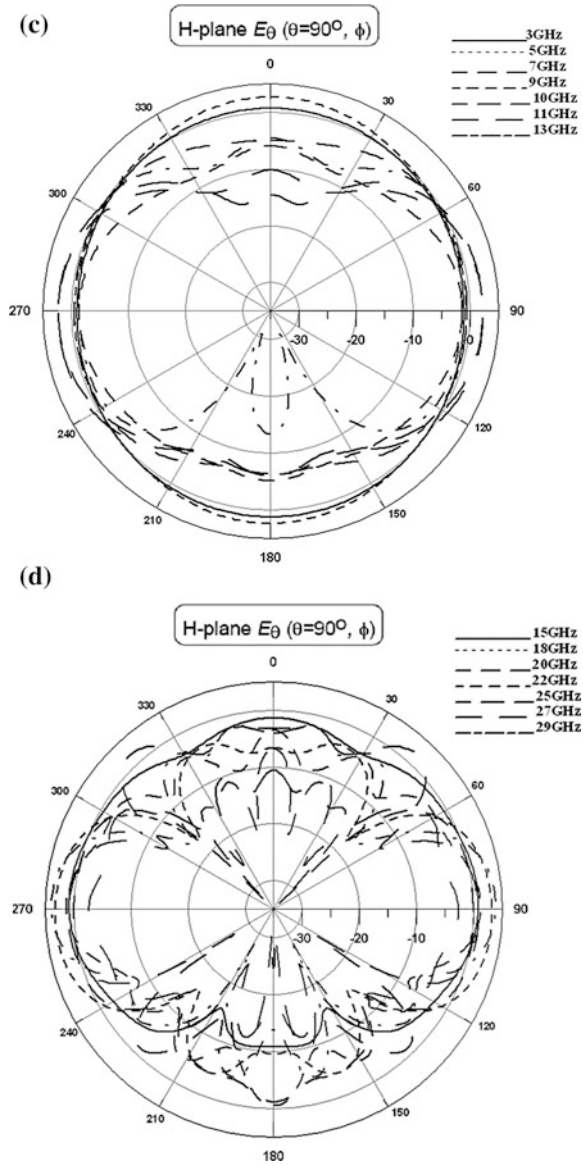


Fig. 5.4 (continued)

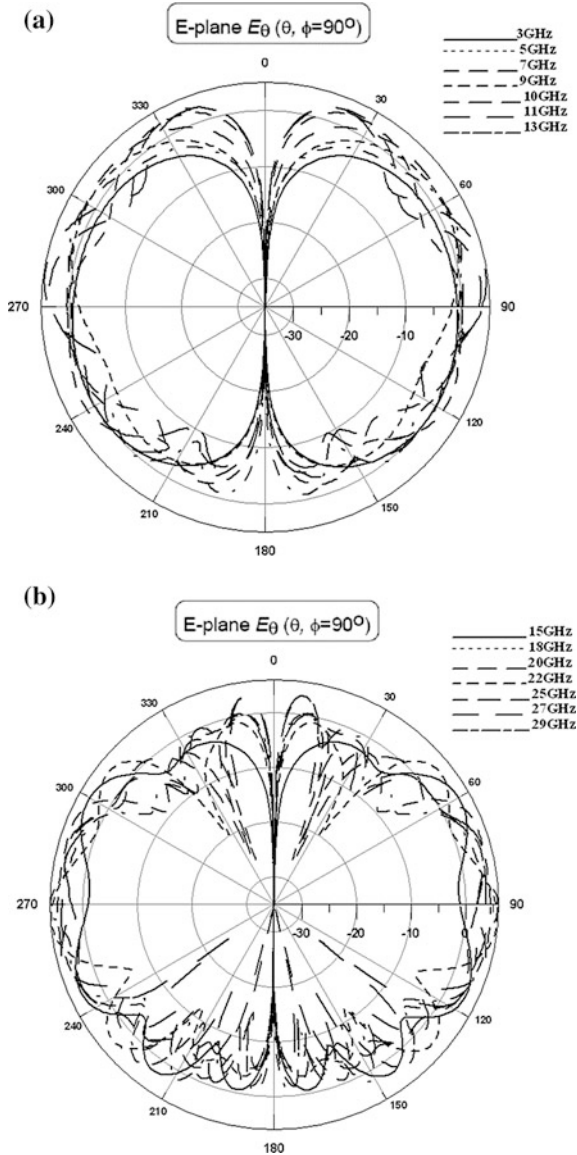


Fig. 5.5 E-plane (a and b) and H-plane (c and d) radiation patterns of the coplanar SWB antenna of Fig. 5.2b

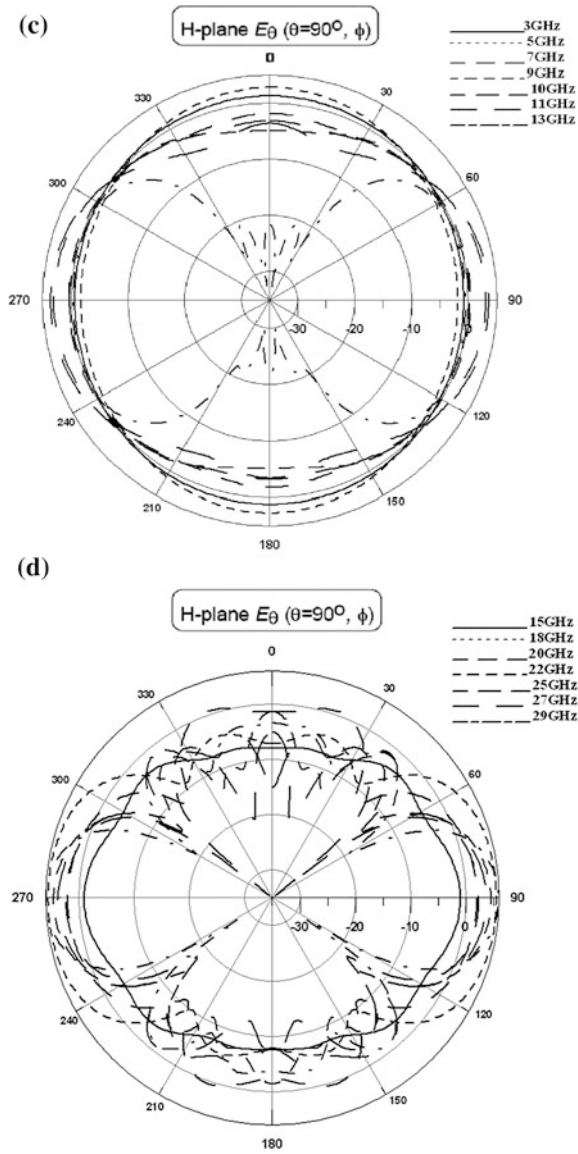


Fig. 5.5 (continued)

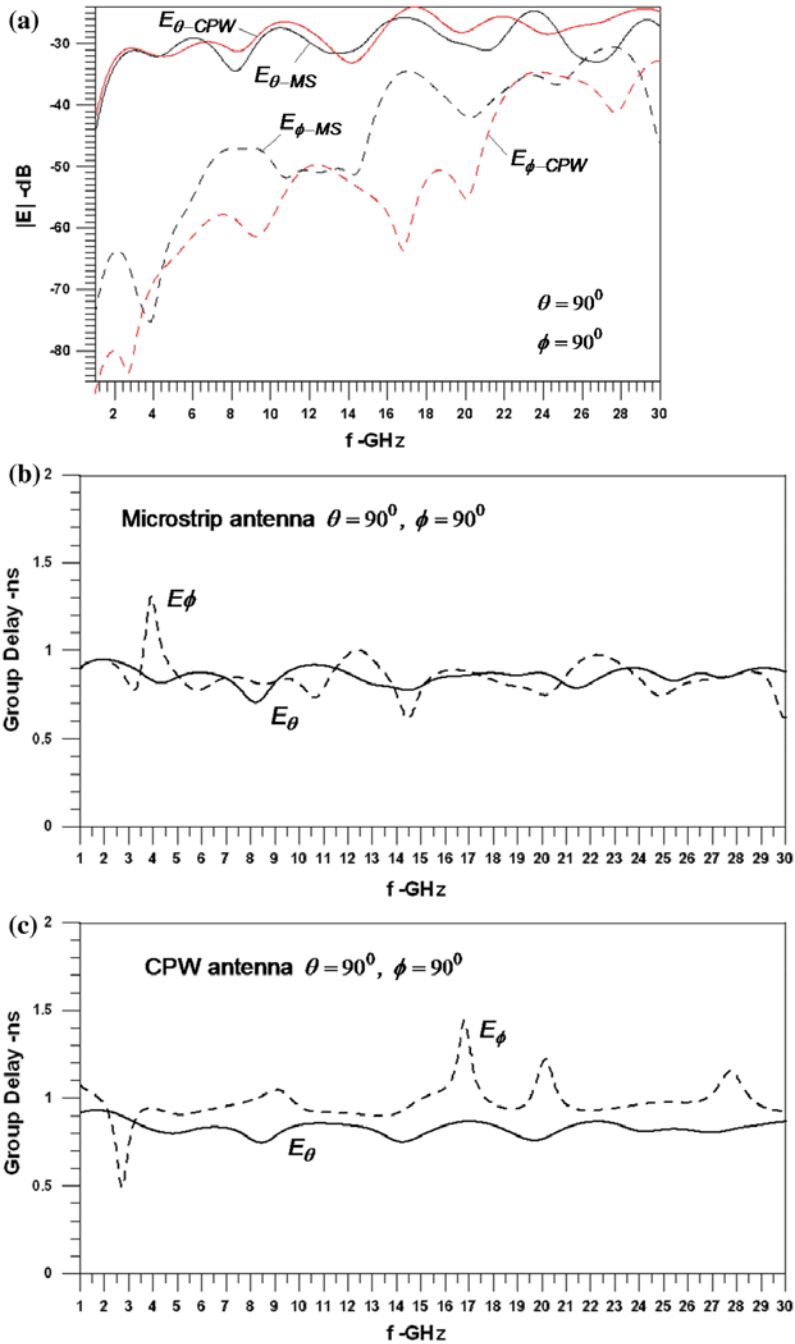


Fig. 5.6 Responses of microstrip and CPW SWB antennas; amplitude responses (a), and group delay of the microstrip (b) and CPW (c) antennas

identical in this narrow frequency range. Note that the cross-polarized level radiated from the microstrip antenna is usually higher than that of the CPW one because this polarization is present in the microstrip feed, but absent from that of the CPW.

In general, the group delay performance is much flatter for vertical than horizontal polarization. The variations are 250 and 700 ps, respectively, for the microstrip antenna (Fig. 5.6b) and 180 and 950 ps, respectively, for the CPW antenna (Fig. 5.6c). This performance is comparable to many other printed-circuit UWB antennas. However, their group delay responses are confined to the much smaller 3–10 UWB GHz frequency range, e.g., [21–24], whereas the results presented here extend such performance to the 3–30 GHz SWB spectrum.

Since the direction of the main beam changes with frequency, it is difficult to present gain plots for SWB antennas. Two approaches are presented here. The first approach displays the vertically polarized gains in specific planes. Figure 5.7a, b shows the maximum E- and H-plane gains of the microstrip and CPW antennas obtained at varying angles. The E-plane patterns are for varying angles θ at $\phi = 90^\circ$, i.e., the yz plane in Fig. 5.1. The H-plane patterns are for varying angles ϕ at $\theta = 90^\circ$, i.e., the xy plane. Both antennas show typical variations in gain performances, and the average gain increases with frequency. Note that gain values below 0 dB in the lower frequency range indicate that the direction of maximum gain might have shifted to a direction different from angles in the E- or H-planes.

As for the second approach, termed “realized gain,” we present the vertically polarized gain in a preferred direction. The related data is shown in Fig. 5.7c as a comparison between the microstrip and CPW antennas for the $\theta = \phi = 90^\circ$ direction. For both antennas, this gain varies rapidly. However, higher gain values are obtained on average for the CPW antenna. It is worthwhile noting that a dip occurs in Fig. 5.7c at 27 GHz for the microstrip antenna. This is the same frequency at which a dual-polarization operation was envisaged previously (c.f. Fig. 5.6a). It is thus obvious that the microstrip antenna’s co-polarized (vertically polarized) gain drops as half of the power is already radiated in the cross-polar (horizontal) direction. However, for remote monitoring or surveillance purposes, it is mostly important that the antenna receives a signal. Its actual strength is of secondary consideration.

This concludes the time-domain performance evaluation of the 3–30 GHz SWB antennas. The concept of the CPW antenna is now extended to 60 GHz.

5.4 Evaluation of the 3–60 GHz CPW Antenna

According to the investigation presented in Fig. 5.3b, lower permittivity substrates and/or reduced substrate heights are required for antennas to work into the millimeter-wave frequency ranges. Thus, the substrate for the 3–60 GHz SWB antenna is selected as RT 5870 with $\epsilon_r = 2.35$, $\tan\delta = 0.0012$, substrate height of

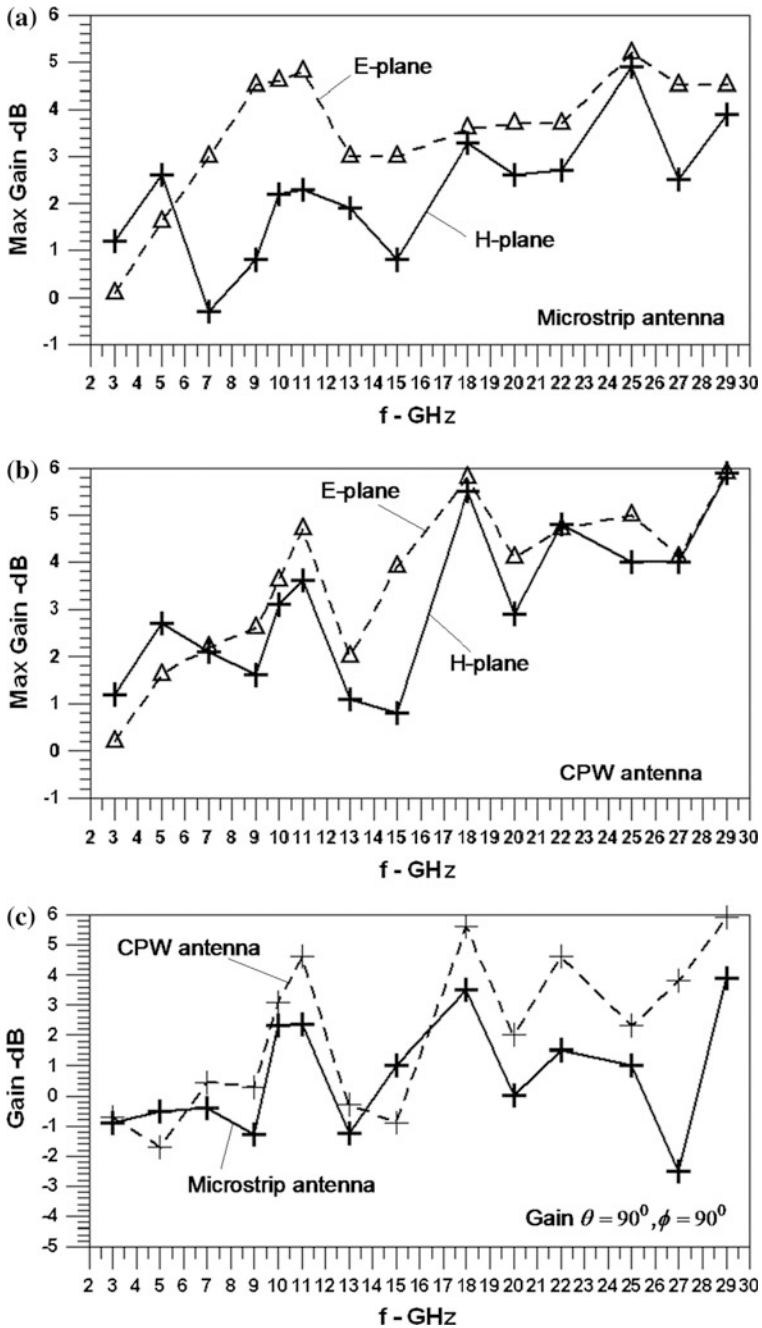
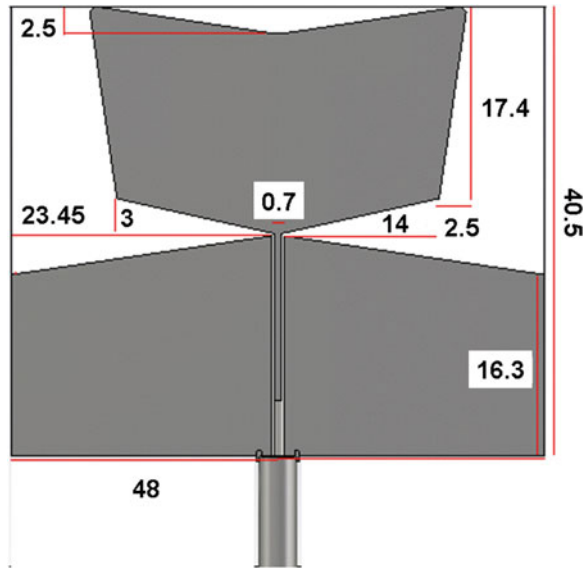


Fig. 5.7 Different gain performances of microstrip and CPW SWB antennas; maximum gain microstrip (a), maximum gain CPW (b), and realized gain for microstrip and CPW antennas (c)

Fig. 5.8 Layout and dimensions (in mm) of printed-circuit 3–60 GHz SWB antenna in CPW technology



0.254 mm, and metallization thickness of 17.5 μm . Moreover, compared to the 3–30 GHz antennas discussed in Sect. 5.3, the feed is changed to reflect a 65 GHz coaxial cable. Figure 5.8 shows the layout and dimensions of the CPW antenna following the design procedure in Sect. 5.2.

Figure 5.9 shows the input reflection coefficient of the CPW antenna of Fig. 5.8, which displays excellent performance between 3.2 and 60 GHz. For validation, the results of the time-domain solver of CST Microwave Studio are compared with those of the frequency-domain (finite element) solver of HFSS. The agreement is close up to 50 GHz, but deviates above that value. These slight discrepancies are attributed to the fact that in HFSS, the highest meshing frequency was set to 50 GHz in order to keep the CPU time to a reasonable limit. The good agreement between the two field solvers validates the approach for the design of printed-circuit SWB antennas and demonstrates the usefulness and application of computational electromagnetics in SWB systems performance evaluation.

Figure 5.10 depicts the E- and H-plane radiation pattern of the CPW SWB antenna for 20 different frequencies between 3 and 60 GHz. These patterns are similar to those of the 3–30 GHz CPW antenna (Fig. 5.5) in the sense that at lower frequencies, the antenna behaves like a monopole, whereas it becomes more directional toward higher frequencies. However, the performance between 15 and 30 GHz is better than that of Fig. 5.5 since the large number of pattern minima occur between 30 and 60 GHz and not, as in Fig. 5.5, between 15 and 30 GHz. This is a result of the lower permittivity and reduced-height substrate selected for the 3–60 GHz design. Again, it is noted that despite the increasing number of minima toward higher frequencies, transmission and reception are maintained in

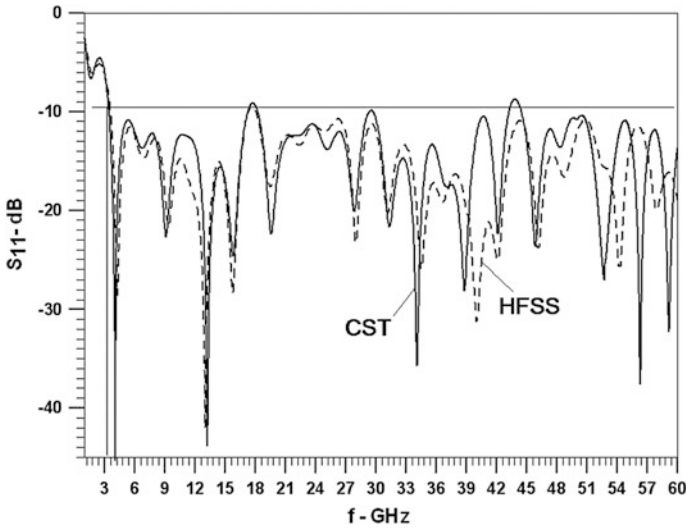


Fig. 5.9 Reflection coefficient in dB of the 3–60 GHz SWB antenna of Fig. 5.8; comparison between CST and HFSS

the directions of $\theta = 90^\circ$ and $\phi = \pm 90^\circ$ at all frequencies. For even higher frequencies, it is expected that the pattern will approach that of a bidirectional LTSA.

The results of the transient analysis, e.g., the levels of co- and cross-polarized fields in the preferred direction of $\theta = \phi = 90^\circ$ are shown in Fig. 5.11a. It is observed that the cross-polarized component increases with frequency, but that even toward 60 GHz, it is more than 10 dB below the co-polarized field. The antenna is thus predominantly vertical polarized, and a dual-polarization application as suggested for the 3–30 GHz microstrip antenna (Fig. 5.6a) is not possible.

The phase information corresponding to the amplitude levels of Fig. 5.11a is displayed as group delay in Fig. 5.11b. The group delay variation for the vertical (co-) polarization is less than 150 ps up to 60 GHz. This is a quite remarkable value considering the bandwidth ratio of 20:1. A much larger variation and several spikes are observed in the group delay of the cross-polar component. It is thus concluded that only the vertical polarization is suitable for pulse transmission or reception in an SWB communication scenario. For simple spectral monitoring applications in the 3–60 GHz range, however, the group-delay performance is of secondary importance.

Finally, the gain performance of the 3–60 GHz SWB antenna is shown as three different traces in Fig. 5.12. As explained in Sect. 5.3, the E-plane curve is the maximum gain obtained in the E-plane at varying angles θ , i.e., the yz plane in Fig. 5.1. The H-plane gain is the maximum gain at varying angles ϕ in the H-plane where $\theta = 90^\circ$. And the third curve shows the gain in the direction of $\theta = \phi = 90^\circ$. In the lower frequency range, this gain can fall below 0 dB as the direction

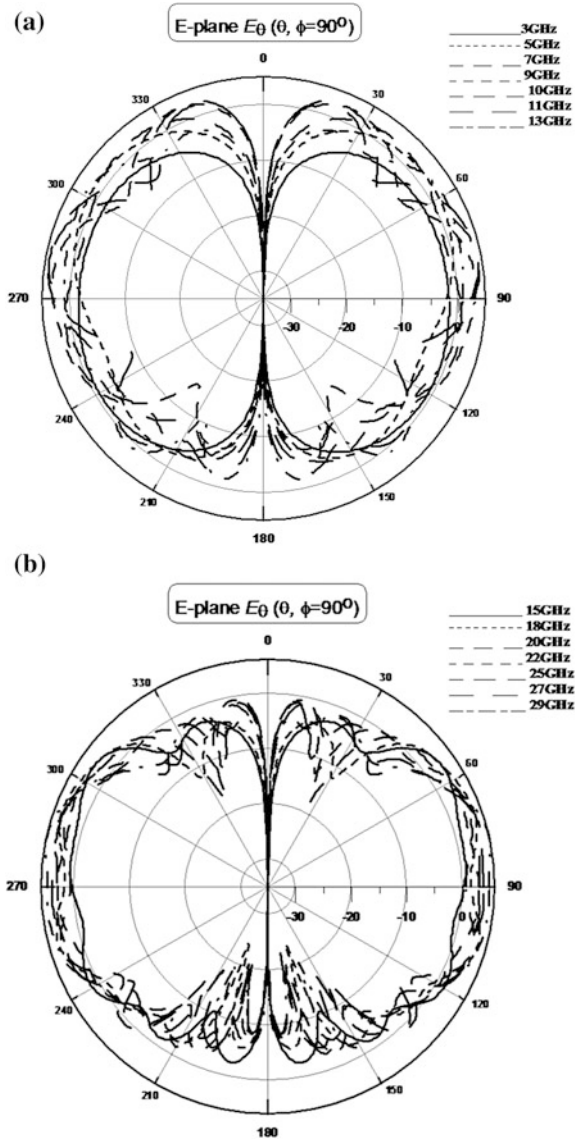


Fig. 5.10 E-plane (a, b, c) and H-plane (d, e, f) radiation patterns of the coplanar SWB antenna of Fig. 5.8

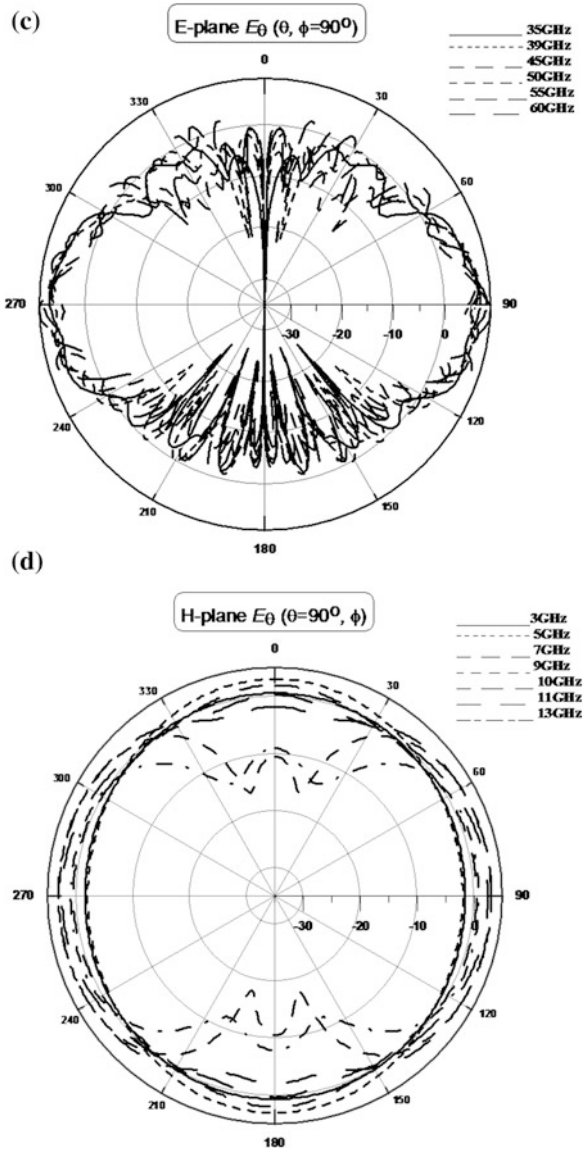


Fig. 5.10 (continued)

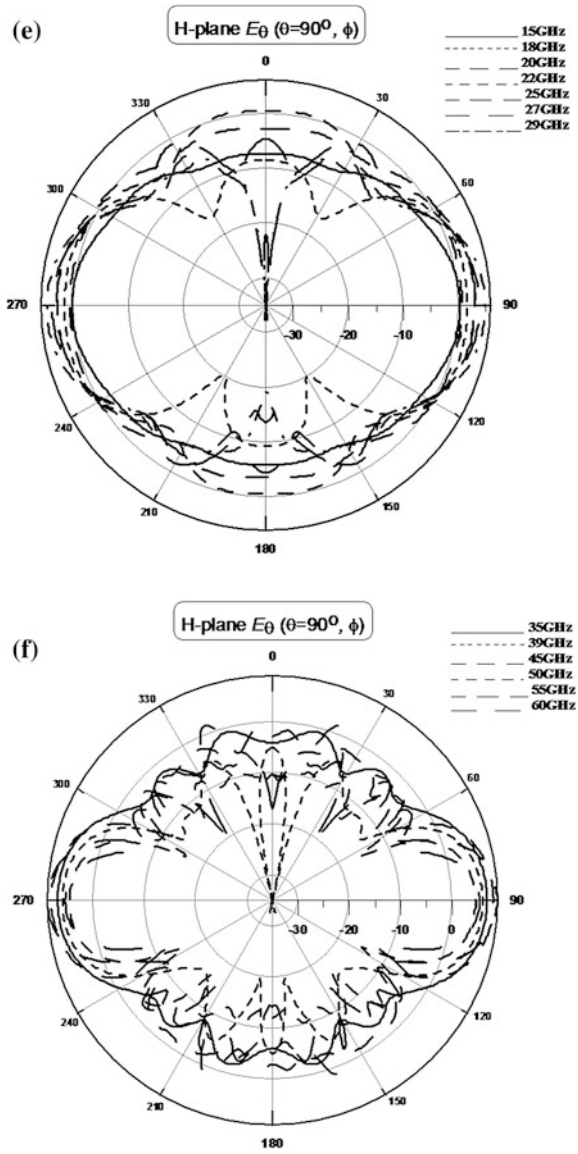


Fig. 5.10 (continued)

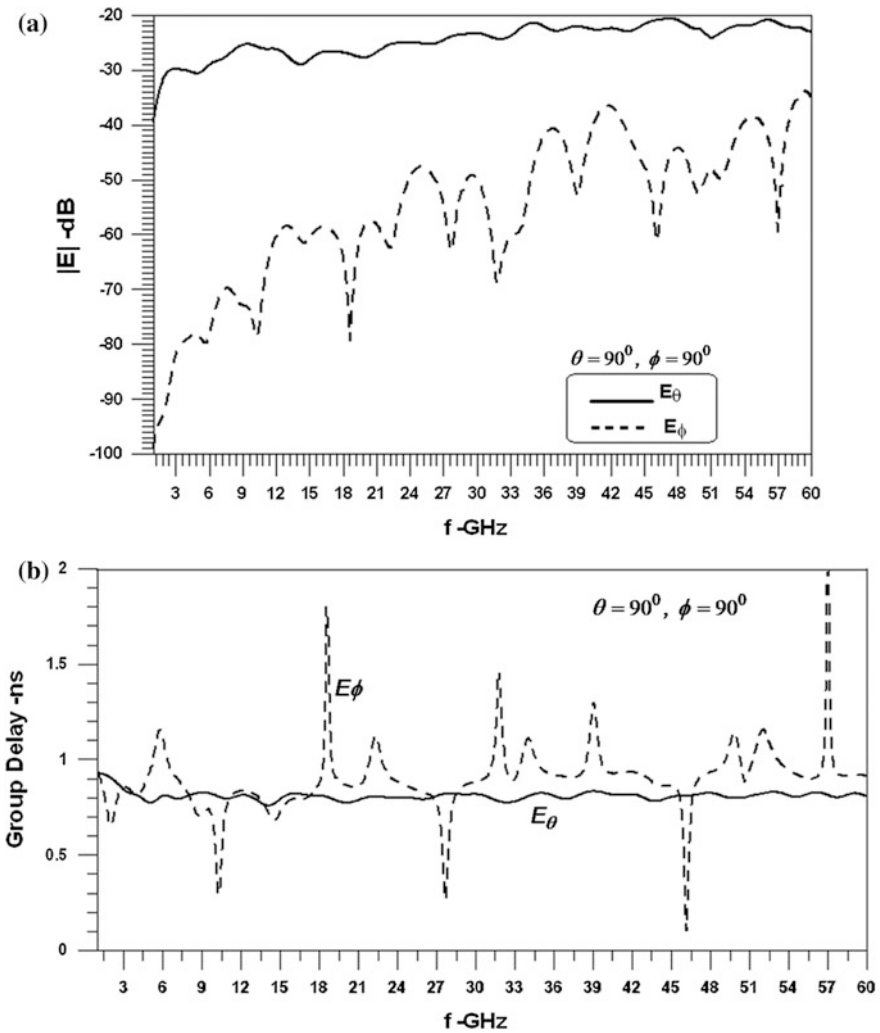


Fig. 5.11 Amplitude responses (a) and group delay performance (b) of co- and cross-polarized electric fields for the coplanar antenna in Fig. 5.8 with probes located at $\theta = \phi = 90^\circ$

of maximum gain changes with frequency, and might not exactly fall in the indicated direction. For frequencies greater than 9 GHz, the maximum H-plane gain is almost identical to that in the direction $\theta = \phi = 90^\circ$. Note that the three gain curves start to align at frequencies above 27 GHz. This confirms that the main direction of radiation is actually that of $\theta = 90^\circ$ and $\phi = 90^\circ$ and, by consideration of symmetry in Fig. 5.8, also that of $\theta = 90^\circ$ and $\phi = -90^\circ$.

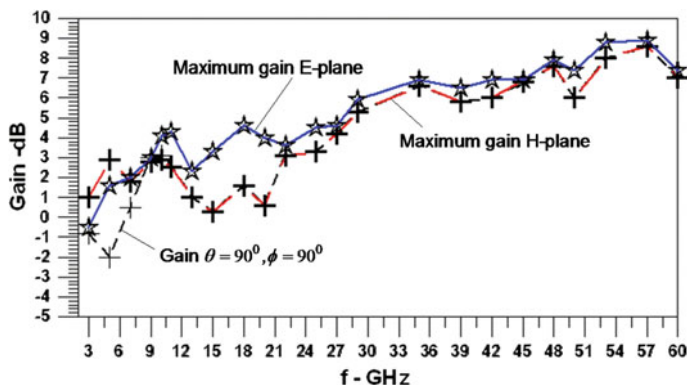


Fig. 5.12 Gain performance of SWB antenna in Fig. 5.8 including maximum gains in E- and H-plane (but varying angles) and gain toward $\theta = \phi = 90^\circ$

5.5 Conclusions

Time-domain modeling and analysis demonstrates that printed-circuit antennas with monopole-like shapes, which have been proposed for the UWB applications between 3.1 and 10.6 GHz, can be extended to cover SWB frequency ranges up to 30 GHz and even up to 60 GHz. The two printed-circuit antennas for 3–30 GHz SWB monitoring applications, as well as the antenna up to 60 GHz, achieve a return loss of 10 dB over the entire bandwidth. Their transient responses in terms of amplitude and group delay performances are acceptable and compare well with other UWB printed-circuit antennas that have been presented previously only for the 3–10 GHz band. However, since the main beam (or possibly multiple beams) changes directions with frequency, the gain of both antennas varies drastically in specific directions and/or planes. Therefore, such antennas are preferred to be mobile when employed in monitoring or surveillance equipment. The 3–30 GHz microstrip antenna shows possibility of dual-polarized applications at around 27 GHz. The 3–30 GHz coplanar antenna demonstrates slightly better amplitude, group delay, and gain performance overall. The 3–60 GHz coplanar antenna on a lower permittivity and thinner substrate presents a viable option for SWB spectral monitoring as demonstrated by performance comparison of two independent field solvers. The time-domain approach is validated by comparison with results from a frequency-domain technique. The investigation shows that time-domain computational electromagnetic codes are indispensable in the performance evaluation and design of UWB and SWB antennas.

Acknowledgments The authors gratefully acknowledge the support for this work from the Natural Sciences and Engineering Research Council of Canada and the TELUS Research Grant in Wireless Communications.

References

1. A.L. Amadjikpè, D. Choudhury, G.E. Ponchak, J. Papapolymerou, Location specific coverage with wireless platform integrated 60 GHz antenna systems. *IEEE Trans. Antennas Propag.* **59**, 2661–2671 (2011)
2. J.D. Brunett, R.M. Ringler, V.V. Liepa, On measurements for EIRP compliance of UWB devices, in *IEEE EMC-S International Symposium Digest* (Chicago, USA, Aug 2005) pp. 473–476
3. C. Yoon, H. Park, W. Lee, M. Shin, J.S. Pak, J. Kim, Power/ground noise immunity test in wireless and high-speed UWB communication system, in *IEEE EMC-S International Symposium Digest* (Detroit, USA, Aug 2008) pp. 1–6
4. H. Kamiya, M. Yamada, M. Tokuda, S. Ishigami, K. Gotoh, Y. Matsumoto, A new method for measuring interference between UWB and wireless LAN systems, in *Proceedings of the International Wireless Communications and Mobile Computing Conference*, (Crete, Greece, Aug 2008) pp. 1106–1111
5. C. Adami, C. Braun, P. Clemens, M. Suhrke, H.U. Schmidt, A. Taenzer, HPM detection system for mobile and stationary use, in *Proceedings of the International Symposium on Electromagnetic Compatibility*, (York, UK, Sep 2011) pp. 1–6
6. O. Lauer, M. Riederer, N. Karoui, R. Vahldieck, E. Keller, J. Fröhlich, Characterization of the electromagnetic environment in a hospital, *Proceedings of the Asia-Pacific Symposium on Electromagnetic Compatibility*, (Singapore, May 2008) pp. 474–477
7. M. Barbiroli, C. Carciofi, D. Guiducci, Assessment of population and occupational exposure to Wi-Fi systems: measurements and simulations. *IEEE Trans. Electromag. Compat.* **53**, 219–228 (2011)
8. J. Zhang, P.V. Orlik, Z. Sahinoglu, A.F. Molisch, P. Kinney, UWB systems for wireless sensor networks. *Proc. IEEE* **97**, 313–331 (2009)
9. J. Yu, Y. Cen, S. Chen, S. Wai, X. Chen, S. Liu, M. Zhou, Y. Gaol, Design of EMC testing equipment for mobile phones, in *Proceedings of the International Conference on Microwave Technology and Computational Electromagnetics*, (Beijing, China, Nov 2009) pp. 192–195
10. C. Hoffmann, P. Russer, A broadband high-dynamic time-domain system for EMI measurements in K-band up to 26 GHz, in *IEEE EMC-S International Symposium Digest*, (Long Beach, USA, Aug 2011) pp. 489–492
11. K. Chung, S. Pyun, J. Choi, Design of an ultrawide-band TEM horn antenna with a microstrip-type balun. *IEEE Trans. Antennas Propagat.* **53**, 3410–3413 (2005)
12. E.S. Pires, P.I.L. Ferreira, G. Fontgalland, M.A.B. de Melo, R.M. Valle, T.P. Vuong, Design of a UWB antenna for sensor and wireless systems applications, in *Proceedings of the IEEE International Conference on Ultra-Wideband*, (Hannover, Germany, Sep 2008) pp. 185–188
13. H.-J. Lam, J. Bornemann, Ultra-wideband printed-circuit antenna in coplanar technology, in *IEEE EMC-S International Symposium Digest*, TU-PM-1-7, (Honolulu, USA, July 2007) pp. 1–4
14. M.A. Peyrot-Solis, G.M. Galvan-Tejada, H. Jardon-Aguilar, Directional UWB planar antenna for operation in the 5–20 GHz band, in *Proceedings of the 17th International Zurich Symposium EMC*, (Singapore, Feb, Mar 2006) pp. 277–280
15. J. Liu, K.P. Esselle, S. Zhong, Creating multiple band notches in an extremely wideband printed monopole antenna, in *Proceedings of the Asia-Pacific Microwave Conference*, (Yokohama, Japan, Dec 2010) pp. 2220–2223
16. K. Rambabu, H.A. Thiart, J. Bornemann, S.Y. Yu, Ultrawideband printed-circuit antenna. *IEEE Trans. Antennas Propagat.* **54**, 3908–3911 (2006)
17. J. Bai, S. Shi, D.W. Prather, Modified compact antipodal vivaldi antenna for 4–50 GHz UWB application. *IEEE Trans. Microwave Theory Tech.* **59**, 1051–1057 (2011)
18. M. Mokhtaari, J. Bornemann, Printed-circuit antennas for 3–30 and 3–60 GHz UWB applications, in *Proceedings of the Asia-Pacific Microwave Conference*, (Yokohama, Japan, Dec 2010) pp. 1922–1925

19. D. Tran, A. Szilagy, I.E. Lager, P. Aubry, L.P. Ligthart, A. Yarovoy, A super wideband antenna, in *Proceedings of the European Conference on Antennas and Propagation*, (Rome, Italy, Apr 2011) pp. 2807–2811
20. T. Hagstrom, S. Lau, Radiation boundary conditions for Maxwell's equations: A review of accurate time-domain formulations. *J. Comput. Math.* **25**, 305–336 (2007)
21. S.H. Choi, J.K. Park, S.K. Kim, J.Y. Park, A new ultra-wideband antenna for UWB applications. *Microwave Opt. Tech. Lett.* **40**(5), 399–401 (2004)
22. T.-G. Ma, C.-H. Tseng, An ultrawideband coplanar waveguide-fed tapered ring slot antenna. *IEEE Trans. Antennas Propag.* **54**, 1105–1110 (2006)
23. Y. Lee, S. Hong, J. Kim, J. Choi, Design of an internal antenna with near-omnidirectional H-plane radiation pattern over ultra-wide bandwidth. *ETRI Journ.* **32**, 62–67 (2010)
24. C.-Y.-D. Sim, W.-T. Chung, C.-H. Lee, Compact slot antenna for UWB applications. *IEEE Antennas Wirel. Comp. Lett.* **9**, 63–66 (2010)